Postprint of: Żak A., Krawczuk M., Skarbek Ł., Palacz M., Numerical analysis of elastic wave propagation in unbounded structures, Finite Elements in Analysis and Design, Vol. 90 (2014), pp. 1-10, DOI: 10.1016/j.finel.2014.06.001

Numerical analysis of elastic wave propagation in unbounded structures

A. Żak[a,], M. Krawczuk[a], Ł. Skarbek[a], M. Palacz[a]

[a] *Gdańsk University of Technology, Faculty of Electrical and Control Engineering, ul. Własna Strzecha 18A, 80-234 Gdańsk, Poland*

Abstract

The main objective of this paper is to show the effectiveness and usefulness of the concept of an absorbing layer with increasing damping (ALID) in numerical investigations of elastic wave propagation in unbounded engineering structures. This has been achieved by the authors by a careful investigation of three different types of structures characterised by gradually increasing geometrical and mathematical description complexities. The analysis included propagation of longitudinal elastic waves in a 1-D semi-infinite isotropic rod, modelled according to the classical 1-mode theory of rods, propagation of coupled shear and flexural elastic waves in a 1-D semi-infinite isotropic beam modelled according to the Timoshenko beam theory, as well as propagation of elastic waves in a 3-D semi-infinite isotropic half-pipe shell modelled by a 6-mode theory of shells. The concept of the ALID has been not only presented by the authors, but certain relations between the ALID properties and the characteristics of propagating elastic waves have been given that can help to maximise the ALID performance in terms of its damping capability. All results of numerical calculations presented by the authors in this work have been obtained by the use of the Time-Domain Spectral Finite Element Method (TD-SFEM).

Keywords: time-domain spectral finite element method, unbounded structures, wave propagation, elastic waves, absorbing layer, structural damping

1. Introduction

Recently various structural health monitoring (SHM) techniques have become the subject of extensive scientific investigations [1]. Among many techniques used for that purpose those based on elastic wave propagation and wave

*Corresponding author

Email addresses: a.zak@ely.pg.gda.pl (A. Żak), markrawc@pg.gda.pl (M. Krawczuk), lskarbek@ely.pg.gda.pl (Ł. Skarbek), m.palacz@ely.pg.gda.pl (M. Palacz)

scattering have become widely exploited both experimentally [2] and numerically [3]. However, in many cases numerical investigations are strongly influenced by scale factors resulting from the fact that the lengths of propagating elastic waves are very often much smaller than characteristic structural dimensions. This usually leads either to large numerical models of millions degrees of freedom in the first case [4, 5] or unwanted boundary effects [6, 7] in the second case, when only selected parts of structures are investigated. In that context numerical techniques enabling one not only to reduce the boundary effects, but also to reduce the size of numerical models, are strongly sought and required.

It should be noted that unwanted wave reflections from boundaries may influence or mask reflections resulting from the presence of structural defects making structural analysis very complex. In the case of numerical models employed to solve various wave propagation problems removal of unwanted boundary reflections is equivalent to representing total radiation outside the area of the study. This problem can be solved by using different methods such as: infinite elements [8], boundary integral methods [9], non-reflecting boundary conditions [10], as well as absorbing layer techniques [11].

Infinite element methods are based on special types of elements with modified properties that are aggregated by standard finite element routines, but used to model the infinite space. The application of infinite elements leads to good results in the case of various static problems, as well as in certain cases of wave propagation problems, these being electromagnetism and acoustics. However, results presented in [12–18] prove that infinite elements are not suitable for a high accuracy removal of unwanted boundary reflections in the case of propagation of guided or bulk waves. Also the area of analysis must be much bigger than the area of investigation, which results in an increase in the number of model degrees of freedom.

On the other hand non-reflecting boundary conditions are in fact special types of boundary conditions used in order to model wave propagation in unbounded media [19]. These techniques are based on extra variables used to approximate the infinite dimensions of the media and can be successfully applied in the case of the Finite Element Method (FEM) or the Finite Difference Method (FDM). The model dimensions remain the same as the area under consideration. These techniques also lead to good results, but they require certain modifications of standard solution procedures applied by the FEM or the FDM.

The technique of absorbing layers allows the absorption of waves that enter the layers. Certain small reflections from the absorbing layers may exist, but their amplitudes can be reduced by correct definition of layer parameters. Two techniques based on the concept of absorbing layers exists in the literature, known as a perfectly matched layer (PML) or an absorbing layer with increasing damping (ALID). Originally the PML was developed and employed in the case of electromagnetic waves [20, 21], but later was extended onto the fields of acoustics [22], seismology [23, 24], as well as onto elastic waves [25–28]. Theoretically waves enter the PML without reflections and decay inside exponentially. In practice due to various model discontinuities, mainly arising and present due to numerical reasons between the area under investigation and the

layer, small reflections can be observed. For this reason a correct definition of PML parameters, such like its length and attenuation, remain essential in order to achieve a proper and efficient model that leads to good results. Contrary to this the ALID utilises the concept proposed in [19]. In this case the absorbing layer is presented by material with its damping properties increasing along the depth of the layer. This method was successfully applied for modelling wave propagation in water [29] and porous media [30].

The main objective of this paper is to show the effectiveness and usefulness of the concept of an absorbing layer with increasing damping (ALID) in numerical investigations of elastic wave propagation in unbounded engineering structures. This has been achieved by the authors by a careful investigation of three different types of structures characterised by their gradually increasing geometrical and mathematical description complexity. The analysis included propagation of longitudinal elastic waves in a 1-D semi-infinite isotropic rod, modelled according to the classical 1-mode theory of rods [31], propagation of coupled shear and flexural elastic waves in a 1-D semi-infinite isotropic beam, modelled according to the Timoshenko beam theory [32], as well as propagation of elastic waves in a 3-D semi-infinite isotropic half-pipe shell modelled by a 6-mode theory of shells [33]. The concept of the ALID has not only been presented by the Authors, but certain relations between the ALID properties and the characteristics of propagating elastic waves have been given that can help to maximise the ALID performance in terms of its damping capability. All results of numerical calculations presented by the Authors in this work have been obtained by the use of the Timed-domain Spectral Finite Element Method (TD-SFEM) [3].

2. Absorbing layer with increasing damping

The concept of an absorbing layer with increasing damping (ALID) is well described in [13], however it should be mentioned at this point that this idea dates back to 1980s [28]. This concept can be explained by considering a simple 1-D equation of motion in the time domain, written for the layer using the FEM convention [34], as:

$$[\mathbf{M}]\{\ddot{q}\} + [\mathbf{C}]\{\dot{q}\} + [\mathbf{K}]\{q\} = \{F\} \tag{1}$$

where $[\mathbf{M}]$, $[\mathbf{C}]$ and $[\mathbf{K}]$ are the characteristic inertia, damping and stiffness matrices, while $\{q\}$ and $\{F\}$ are the vectors of nodal displacements and forces dependent on the x co-ordinate only. The symbols $\dot{\square} = \frac{d}{dt}$ and $\ddot{\square} = \frac{d^2}{dt^2}$ denote the first and second time derivatives, respectively.

Under assumption that the damping matrix $[\mathbf{C}]$ within the ALID is a linear combination of both the inertia $[\mathbf{M}]$ and the stiffness $[\mathbf{K}]$ matrices, as well as that harmonic waves can propagate only along the x-axis, it can be written that:

$$[\mathbf{C}] = a(x)[\mathbf{M}] + b(x)[\mathbf{K}], \quad \{q\} = \{\hat{q}\}e^{-i\omega t}e^{ikx} \tag{2}$$

where ω and k are the angular frequency and the wave number, while $a(x)$ and $b(x)$ are certain smooth scaling functions that vary along the depth of the ALID in the following manner:

$$a(0) = b(0) = 0, \quad a(l) = b(l) = 1 \tag{3}$$

where $x = 0$ corresponds to the structure-layer interface and $x = l$ to the full length of the layer. The symbol $i = \sqrt{-1}$ denotes the imaginary unit, while $\{\hat{q}\}$ is the vector of nodal displacement amplitudes.

After substitution of relations (2) into (1) and necessary rearrangement of terms the original equation of motion in the time domain (1) can represented in the frequency domain as:

$$-\rho\left(1 + i\frac{a(x)}{\omega}\right)[\tilde{\mathbf{M}}]\omega^2\{q\} + E\left(1 - i\omega b(x)\right)[\tilde{\mathbf{K}}]\{q\} = \{F\} \tag{4}$$

with $[\mathbf{M}] = \rho[\tilde{\mathbf{M}}]$ and $[\mathbf{K}] = E[\tilde{\mathbf{K}}]$, and where ρ and E are the frequency independent material density and elastic modulus, respectively.

From the equation of motion (4) it arises that both density ρ and elastic modulus E can be considered as frequency dependant within the ALID:

$$\rho(\omega) = \rho\left(1 + i\frac{a(x)}{\omega}\right), \quad E(\omega) = E\left(1 - i\omega b(x)\right) \tag{5}$$

what allows to express the frequency dependant wave number $k(\omega)$ as:

$$k^2(\omega) = \omega^2\frac{\rho(\omega)}{E(\omega)} = \omega^2\frac{\rho}{E}(c + id) \tag{6}$$

where:

$$c = \frac{1 - a(x)b(x)}{1 + b^2(x)\omega^2}, \quad d = \frac{a(x) + b(x)\omega}{\omega + b^2(x)\omega^3} \tag{7}$$

Based on relations (7) it can be noted that the wave number $k(\omega)$ is complex with its real and imaginary part remaining positive in the case of elastic waves propagating within the ALID in the positive direction [13]. All such waves are attenuated and their wave numbers vary over the length of the layer.

It should be mentioned here that the part of the damping matrix $[\mathbf{C}]$ proportional to the stiffness matrix $b(x)[\mathbf{K}]$ strongly affects numerical solving of the equation of motion (1). In a general case of the TD-SFEM and problems related with propagation of elastic waves the explicit scheme of central differences is commonly used [3], as the scheme can take full advantage of the diagonal (1-D or 2-D problems) or semi-diagonal (3-D problems) forms of the characteristic inertia $[\mathbf{M}]$ and preferably damping $[\mathbf{C}]$ matrices. However, the part of the damping matrix $b(x)[\mathbf{K}]$ is consistent or full and cannot be effectively diagonalised in this case. Moreover, it also strongly affects the stability of the central difference scheme significantly increasing its minimal time step. On the other hand the part of the damping matrix $[\mathbf{C}]$ proportional to the inertia matrix, i.e.

$a(x)[\mathbf{M}]$, is practically free of these drawbacks. For those reasons the damping matrix $[\mathbf{C}]$ is usually assumed in the form:

$$[\mathbf{C}] = a(x)[\mathbf{M}], \quad b(x) = 0 \tag{8}$$

It can be further assumed that the functions $a(x)$ can be expressed as:

$$a(x) = 10^{\alpha} x^{\beta}, \quad \alpha, \beta > 0 \tag{9}$$

which allows to express relation (6) is a simplified form:

$$k^2(\omega) = \omega^2 \frac{\rho}{E} \left(1 + i \frac{10^{\alpha} x^{\beta}}{\omega} \right) \tag{10}$$

In the remaining part of this paper the damping matrix $[\mathbf{C}]$ proportional only to the inertia matrix $[\mathbf{M}]$ is considered, which following relation (9) can be presented as:

$$[\mathbf{C}] = 10^{\alpha} x^{\beta} [\mathbf{M}], \quad x \in [0, l] \tag{11}$$

Appropriate selection of the values of α and β parameters, as well as the length l of the ALID, has a great influence on the layer damping properties. In the opinion of the authors these values should stay as closely correlated with the characteristics of propagating elastic waves in order to serve as general guidelines in numerical calculations, as it is presented in the following sections of this paper.

3. Numerical simulations

All results of numerical simulations presented in this paper were obtained by the use of the TD-SFEM [3]. The results were divided into three parts. In all cases considered hereafter appropriate spectral finite elements were employed, built based on the 5-th order Lobatto approximation polynomials [3]. In all these cases the associated equations of motion were solved by the explicit scheme of central differences with the diagonal (1-D or 2-D problems) or semi-diagonal (3-D problems) inertia $[\mathbf{M}]$ and damping $[\mathbf{C}]$ characteristic matrices [3]. Numerical calculations were carried out assuming isotropic material properties. For that purpose the following material properties of an aluminium alloy were used: elastic modulus $E = 72.5$ GPa, Poisson's ratio $\nu = 0.33$ and material density $\rho = 2900$ kg/m^3.

3.1. 1-D semi-infinite isotropic rod

The geometry of a semi-infinite isotropic rod under investigation is presented in Fig. 1. The assumed length of the rod is $L = 1.5$ m, while the length of the ALID, representing the part of the rod extending to infinity, is denoted as l and is assumed as varying. The diameter of the rod is $d = 2r = 10$ mm. The rod was modelled by 75 spectral finite elements defined according to the classical 1-mode theory of rods [31].

As an excitation force an 8-pulse sine signal modulated by the Hann window was used, acting at the origin of the co-ordinate system, as presented in Fig. 1. The amplitude of the excitation force acting along x-axis was 1 N, while its frequency was 200 kHz. The free type of boundary conditions was used. The total calculation time covered 500 μs and was divided into 2500 time steps.

It should be noted here that according to the applied classical 1-mode theory of rods [31] symmetric (longitudinal) elastic waves propagating within the rod are non-dispersive. Their phase and group velocities c_p and c_g are constant and equal to 5000 m/s in the current case. That fact greatly simplified the analysis that covered the influence of the α and β parameters on the damping capability of the ALID, noted as δ. This capability was expressed in terms of the ratio of energy E_1 to energy E_2 calculated for the same longitudinal displacement component signal $u_x(x,t)$ at two selected time instances t_1 and t_2 before entering and after leaving the layer:

$$\delta = 10 \log_{10} \frac{E_1}{E_2} \tag{12}$$

with:

$$E_1 = \sum_{i=1}^{N} |u_x(x_i, t_1)|^2, \quad E_2 = \sum_{i=1}^{N} |u_x(x_i, t_2)|^2 \tag{13}$$

where N is the total number of degrees of freedom of the rod numerical model. For calculations of the energies E_1 and E_2 the FFT of signals $u_x(x_i, t_1)$ and $u_x(x_i, t_2)$ were employed.

In the case of the rod under consideration the time t_1 was selected as 40 μs. That enabled the complete formation of the excitation signal, which length λ was 0.2 m. The time t_2 was selected as 500 μs. The selected values of t_1 and t_2 correspond to wave propagation distances of 0.2 m and 2.5 m.

As the first the influence of the values of the α and β parameters was analysed on the damping capability of the layer δ. The length l of the ALID was an additional parameter of the analysis. Various values of the α and β parameters

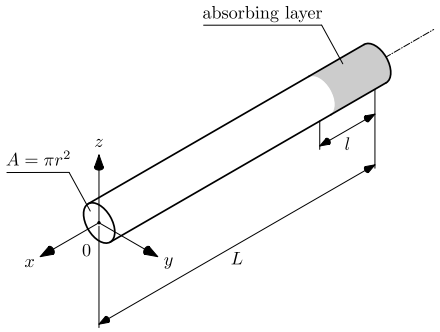

Figure 1: Geometry of an isotropic rod/beam with an absorbing layer.

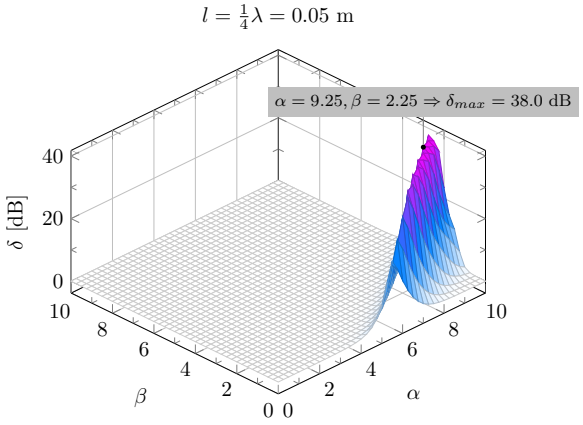

Figure 2: Damping capability δ as a function of α and β parameters for an absorbing layer of 0.05 m.

were tested within the range from 0 to 10 at 41 uniformly distributed discrete points. The results obtained are presented in Figs. 2–5.

It can be immediately noted that the values of the α and β parameters must be very carefully selected and closely correlated not only with the length of propagating elastic waves λ, but also with the length l of the ALID. It can be also seen that in a wide range of their values the ALID has practically no damping capability. This capability arises in a narrow band around certain values of the α and β parameters. For obvious reasons an increase in the length l of the ALID extends the effective damping ability of the layer onto a wider range of the values of the α and β parameters.

The least effective damping was observed when the length l of the ALID was a quarter of the length of propagating elastic waves λ, as seen from Fig. 2. In this case the maximum value of the damping effectiveness δ reached 38.0 dB for the values of the α and β parameters 9.25 and 2.25, respectively. In comparison to that the most effective damping was achieved when the length l of the ALID was double the length of propagating elastic waves λ, as seen from Fig. 5. In this case the maximum value of the damping effectiveness δ reached 42.8 dB for the values of the α and β parameters 6.75 and 3.0, respectively.

It should be noted that an increase in the length l of the ALID resulted in a decrease in the values of the α and β parameters corresponding to the layer maximum damping capacity δ, as long as the length l of the ALID did not exceed the length of propagating elastic waves λ, as presented in Figs. 2–4 and Fig. 5. However, from a computational point of view the length l of the ALID should be selected as an optimal minimum. Therefore in the following cases discussed in this paper this length was always selected as equal to, or double, the length of propagating elastic waves λ.

As the second wave propagation patterns were investigated. They were calculated and obtained for the same rod at selected values of the α parameter.

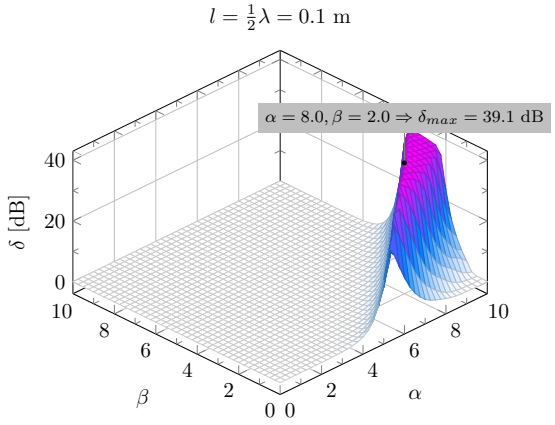

Figure 3: Damping capability δ as a function of α and β parameters for an absorbing layer of 0.1 m.

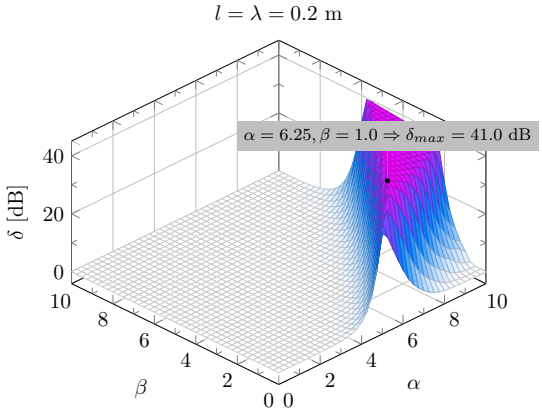

Figure 4: Damping capability δ as a function of α and β parameters for an absorbing layer of 0.2 m.

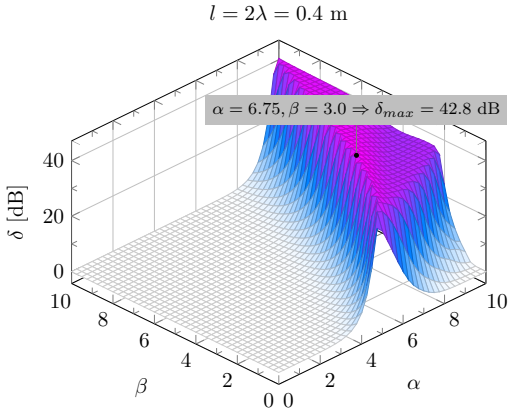

Figure 5: Damping capability δ as a function of α and β parameters for an absorbing layer of 0.4 m.

Following the results presented in Fig. 5 the value of the β parameter was kept constant and equal to 3, while the length of the absorbing layer l was assumed as double the length of propagating elastic waves λ. The damping capability δ was calculated based on the same formula (12). The results obtained are presented in Figs. 6–9.

It can be seen that for the given length l of the ALID ($l = 2\lambda = 0.4$) the value of the α parameter has a strong influence of the wave propagation patterns. It should be noticed that a small variation in this parameter has a dramatic consequence on the performance of the layer. When the value of the α parameter is equal to 5 the ALID has virtually no damping capability and the value of the damping effectiveness δ is only 1.1 dB, as seen in Fig 6. However for the α parameter equal to 6 this effectiveness increases to 11.0 dB, while for the α parameter equal to 7 it reaches 42.0 dB to drop down to 37.7 dB for the α parameter equal to 8, as presented in Figs. 7–9.

3.2. 1-D semi-infinite isotropic beam

The analysis of propagation of bending elastic waves is much more complex. In order to perform this analysis the classical 1-mode theory of rods [31] was replaced by the 2-mode Timoshenko theory of beams [32]. In this theory two independent wave propagation modes can be observed that are characterised by different propagation velocities. These are the primary anti-symmetric (flexural) mode A_0 and the primary anti-symmetric shear mode SH_1 [3].

In the current case the geometry of a semi-infinite isotropic beam under investigation represents the same Fig. 1. However, the assumed length of the beam is $L = 2.0$ m. As before the length of the ALID, representing the part of the beam extending to infinity, and denoted as l, is assumed as varying. The diameter of the beam is also $d = 2r = 10$ mm. The beam was modelled by 100 spectral finite elements defined according to the 2-mode Timoshenko theory of beams [32]. The form and the amplitude of the excitation acting along z-axis

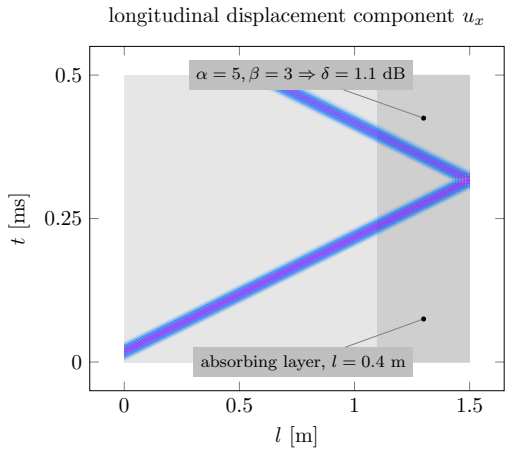

Figure 6: Wave propagation patterns for the longitudinal displacement component u_x of longitudinal elastic waves propagating within an isotropic rod with an absorbing layer ($\alpha = 5, \beta = 3, l = 0.4$ m).

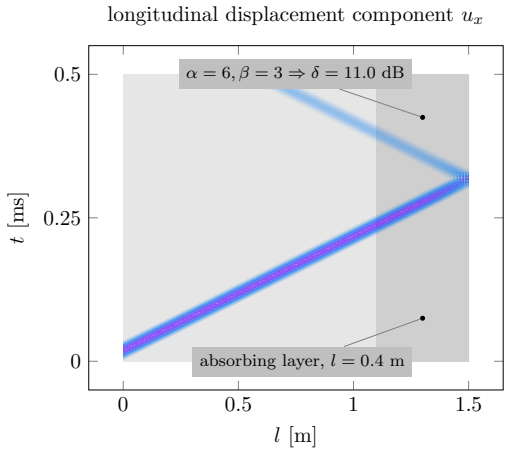

Figure 7: Wave propagation patterns for the longitudinal displacement component u_x of longitudinal elastic waves propagating within an isotropic rod with an absorbing layer ($\alpha = 6, \beta = 3, l = 0.4$ m).

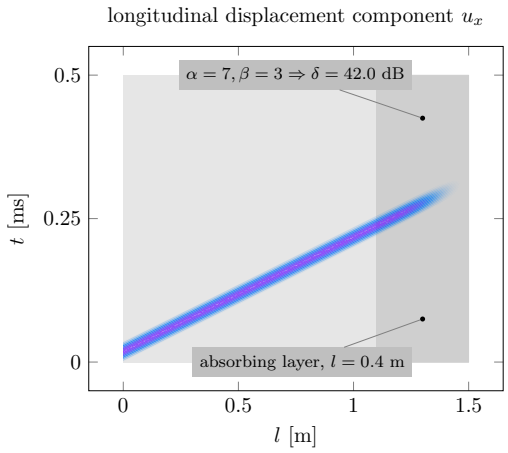

Figure 8: Wave propagation patterns for the longitudinal displacement component u_x of longitudinal elastic waves propagating within an isotropic rod with an absorbing layer ($\alpha = 7, \beta = 3, l = 0.4$ m).

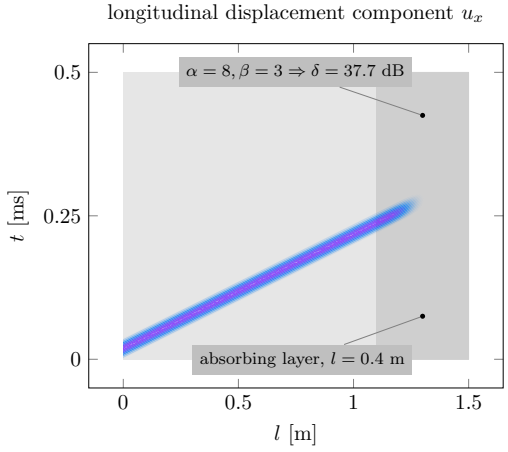

Figure 9: Wave propagation patterns for the longitudinal displacement component u_x of longitudinal elastic waves propagating within an isotropic rod with an absorbing layer ($\alpha = 8, \beta = 3, l = 0.4$ m).

were the same, while its frequency was selected as 100 kHz. The free type of boundary conditions was used. The total calculation time covered 1000 μs and was divided into 5000 time steps.

Because of the dispersive nature of the elastic waves propagating within the beam under investigation their phase and group velocities are different and frequency dependent. For the given excitation frequency of 100 kHz the group velocities of the primary flexural mode A_0 and the primary anti-symmetric shear mode SH_1 can be identified as 2750 m/s and 4900 m/s, both calculated based on the applied 2-mode Timoshenko theory of beams. As a consequence of different propagation velocities the two modes form two signals of different lengths λ_1 and λ_2 equal to 0.22 m and 0.39 m, respectively. This is well seen in Figs. 10–17.

It can be expected that because of the complexity of wave propagation phenomena, as well as the presence of two coupled wave propagation modes A_0 and SH_1, the appropriate selection of the α and β parameters is less obvious. However, it can be noticed that also in this case the length l of the ALID should be closely correlated with the length of propagating waves. Moreover, the results presented in Figs. 10–17 suggest that the length of the layer l should be selected based on the longest waves propagating λ_2. In the current case these are the waves associated with the anti-symmetric shear mode SH_1.

Results presented in Figs. 10–13 indicate that when the length l of the ALID is selected as equal to the longest waves propagating within the beam λ_2 the values of the α and β parameters have great influence on the the damping effectiveness. It can also be noticed from Fig. 10 that for the values of the α and β parameters equal to 5 and 3 the damping capability δ of the ALID can be negative in the case of the longitudinal displacement component u_x. This unusual physical behaviour is a direct consequence of the mode coupling and conversion.

It is well seen that as a result of the excitation both A_0 and SH_1 wave modes propagate together. Due to the coupling between the modes, which originates from shear deformation during wave motion, each boundary reflection of either A_0 and SH_1 mode results in simultaneous generation of both these modes. During the reflection of the incident A_0 mode, the amplitude of the longitudinal component u_x of the generated SH_1 increases at the cost of the transverse component u_r of the same incident A_0 mode, as illustrated by Fig. 11.

On the other hand Fig. 12 and 13 show that the damping capability δ of the ALID, for its current length l, can reach as much as 38.7 dB, for the longitudinal displacement components u_x, and 33.8 dB, for the transverse displacement component u_r, for the values of the α and β parameters equal to 6 and 1.

It is interesting to note that the results presented in Figs. 10–13 correspond well to the results discussed previously and presented in Figs. 6–9. So, when the length l of the ALID is increased to double the length of the longest waves propagating within the beam λ_2 the overall damping effectiveness δ of the ALID is also increased, however, the values of the α and β parameters must be chosen appropriately in order to maximise the layer performance.

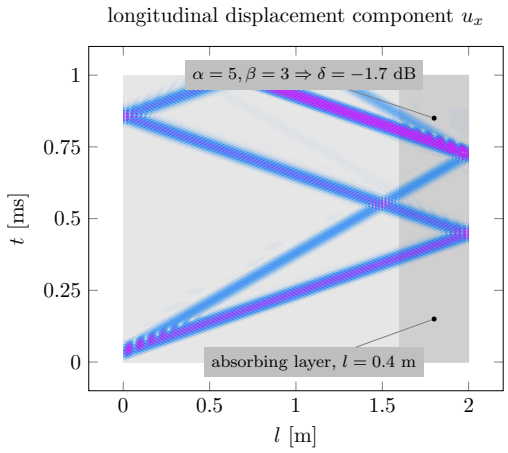

Figure 10: Wave propagation patterns for the longitudinal displacement component u_x of flexural elastic waves propagating within an isotropic beam with an absorbing layer ($\alpha = 5, \beta = 3, l = 0.4$ m).

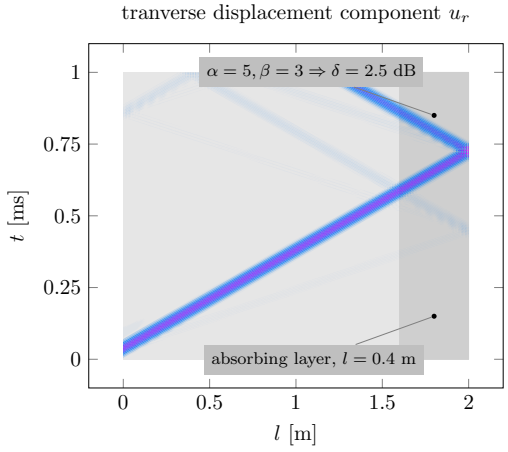

Figure 11: Wave propagation patterns for the transverse displacement component u_r of flexural elastic waves propagating within an isotropic beam with an absorbing layer ($\alpha = 5, \beta = 3, l = 0.4$ m).

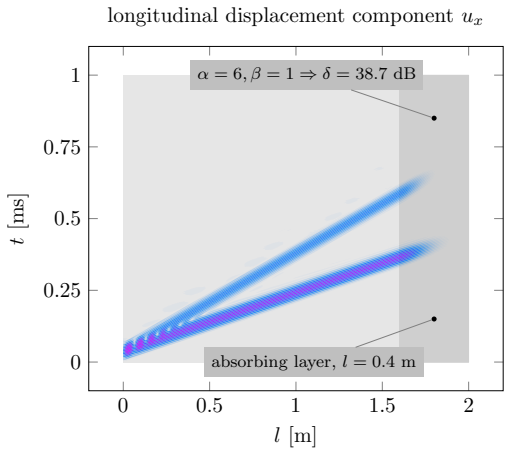

Figure 12: Wave propagation patterns for the longitudinal displacement component u_x of flexural elastic waves propagating within an isotropic beam with an absorbing layer ($\alpha = 6, \beta = 1, l = 0.4$ m).

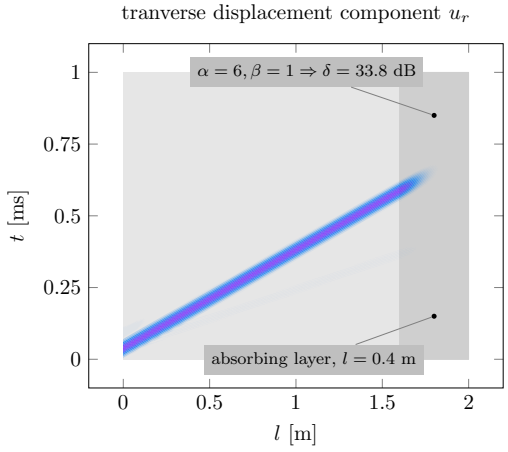

Figure 13: Wave propagation patterns for the transverse displacement component u_r of flexural elastic waves propagating within an isotropic beam with an absorbing layer ($\alpha = 6, \beta = 1, l = 0.4$ m).

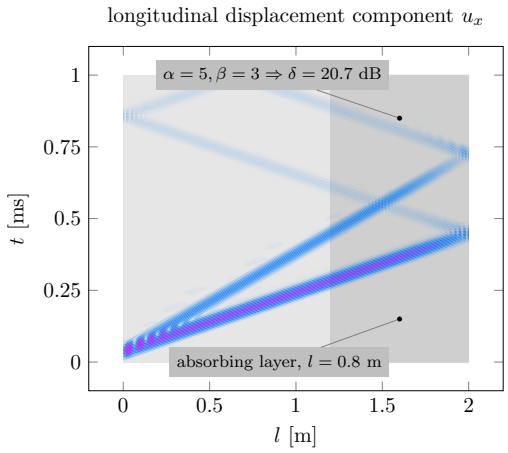

Figure 14: Wave propagation patterns for the longitudinal displacement component u_x of flexural elastic waves propagating within an isotropic beam with an absorbing layer ($\alpha = 5, \beta = 3, l = 0.8$ m).

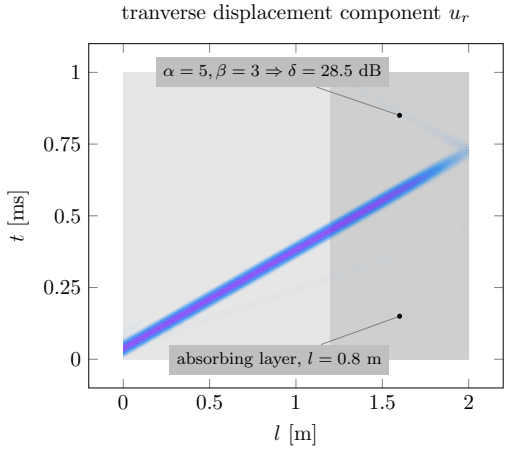

Figure 15: Wave propagation patterns for the transverse displacement component u_r of flexural elastic waves propagating within an isotropic beam with an absorbing layer ($\alpha = 5, \beta = 3, l = 0.8$ m).

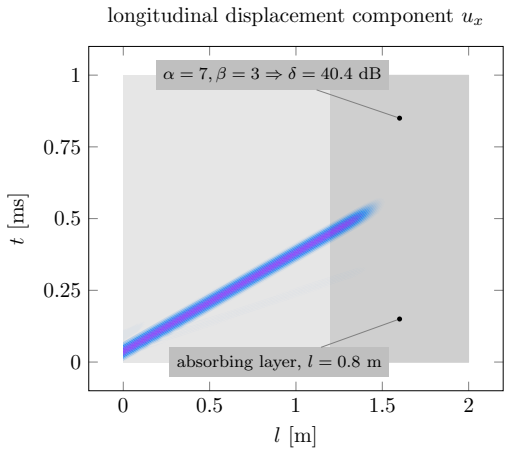

Figure 16: Wave propagation patterns for the longitudinal displacement component u_x of flexural elastic waves propagating within an isotropic beam with an absorbing layer ($\alpha = 7, \beta = 3, l = 0.8$ m).

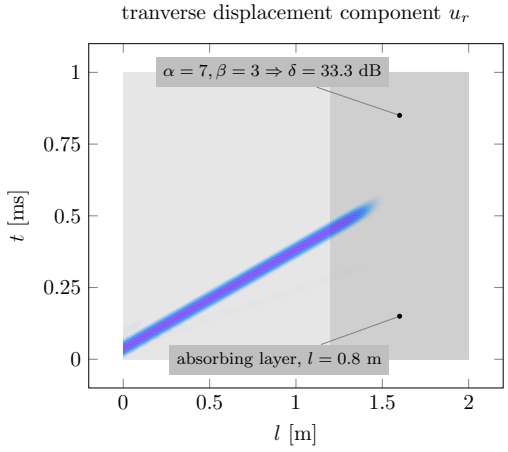

Figure 17: Wave propagation patterns for the transverse displacement component u_r of flexural elastic waves propagating within an isotropic beam with an absorbing layer ($\alpha = 7, \beta = 3, l = 0.8$ m).

3.3. 3-D semi-infinite isotropic half-pipe shell

As the last a 3-D semi-infinite half-pipe shell was investigated. In this case the geometrical and mathematical description complexity of the shell is highest, so are the phenomena associated with propagation of elastic waves within. For this reason the shell was modelled according to a 6-mode theory of shells [33]. In a general case this theory allows propagation of six independent wave modes that are characterised by different propagation velocities. These are two anti-symmetric (flexural) modes A_0 and A_1, two symmetric (longitudinal) modes S_0 and S_1, as well as two shear modes SH_0 (symmetric) and SH_1 (anti-symmetric) [3]. However, in practice only selected wave propagation modes can be observed dependent on the frequency spectrum of structural excitation.

The geometry of a 3-D semi-infinite isotropic half-pipe shell under investigation is presented in Fig. 18. The assumed length of the shell is $L = 0.5$ m. As previously the length of the ALID, representing the part of the shell extending to infinity, is l. The radius of the half-pipe shell is $R = 1$ m, while its thickness is $h = 10$ mm. The half-pipe shell was modelled by 2,236 spectral finite elements defined according to the 6-mode theory of shells [33]. The form and the amplitude of the excitation, acting at point P in the direction of the z-axis, was modified to cover only 4 pulses, while the excitation frequency was selected as 75 kHz. The free type of boundary conditions was used. The total calculation time covered 400 μs and was divided into 8000 time steps.

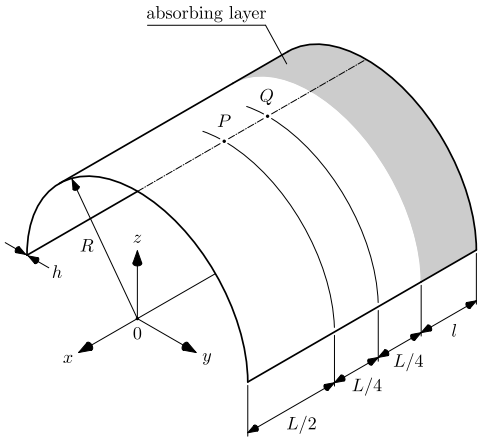

Figure 18: Geometry of an isotropic half-pipe shell with an absorbing layer.

As before the elastic waves propagating within the shell are dispersive in nature and their phase and group velocities are different and frequency dependent. For the given excitation type and frequency of 75 kHz only two wave propagation modes are observable. The group velocities of the primary flexural mode A_0 and the primary symmetric shear mode SH_0 can be identified as 2095 m/s and 3065 m/s, both calculated based on the applied 6-mode theory of shells. Yet again as a consequence of different propagation velocities the two

modes form two signals of different lengths λ_1 and λ_2 equal to 0.11 m and 0.16 m, respectively.

In the case under consideration the effectiveness of the ALID is demonstrated by results of numerical simulation presented in Fig. 19. Following the results of numerical simulations obtained in the case of the rod and beam the values of the α and β parameters were selected as equal to 7 and 3. At the same time the length l of the ALID was selected as double the length of the longest waves that can propagate within the shell $l = 2\lambda_2 = 0.32$ m. It was expected by the authors that for the values of the ALID parameters the damping effectiveness of the ALID should be optimal.

The results shown in Fig. 19 illustrate snapshots of the obtained wave propagation patterns within the 3-D isotropic half-pipe shell without or with the ALID, and calculated at different time instances. In Fig. 19 the ALID was presented as separated in order to improved the legibility of this figure. Due to the geometry of the shell the wave propagation patterns calculated and next presented in Fig. 19 were based on the signal amplitude $A = \sqrt{u_x^2 + u_y^2 + u_z^2}$ rather than on each particular displacement component u_x, u_y or u_z.

It can be clearly seen that the presence of the ALID significantly changes wave propagation patterns. Appropriate selection of the ALID parameters allows for removing any unwanted boundary reflections in the case of semi-infinite boundary conditions. The value of the damping effectiveness δ was not evaluated in this case due to geometrical complexity of the structure, however, the results of the analysis are supplemented by Figs. 20 and 21. They represent two time responses of the shell obtained in the case of the transverse displacement component u_z. The time responses were measured at point Q, as presented in Fig. 18.

It can be clearly seen from Figs. 20 and 21 that the use of the ALID efficiently eradicates all unnecessary boundary reflections, which presence would indicate the finite dimensions of the structure under investigation, as it is shown in Fig. 20. The only boundary reflections present and shown in Fig. 21 are those related with the remaining free boundaries of the shell. This can be noticed based on a comparison of the results presented in Fig. 19 with results presented in Figs. 20 and 21. It is also evident from Fig. 21 that there are no reflection originating from the ALID itself as a result of the incompatibility of mechanical impedance between the structure and the layer.

4. Conclusions

Nowadays numerical simulations play a very important role in engineering sciences as a source of very valuable information about structural behaviour. Therefore it is very important to develop and test more efficient and more sophisticated models that enable their users a deeper insight into simulated phenomena. Problems related with propagation of elastic waves in semi-infinite or infinite structural elements remain not only very important, but also very

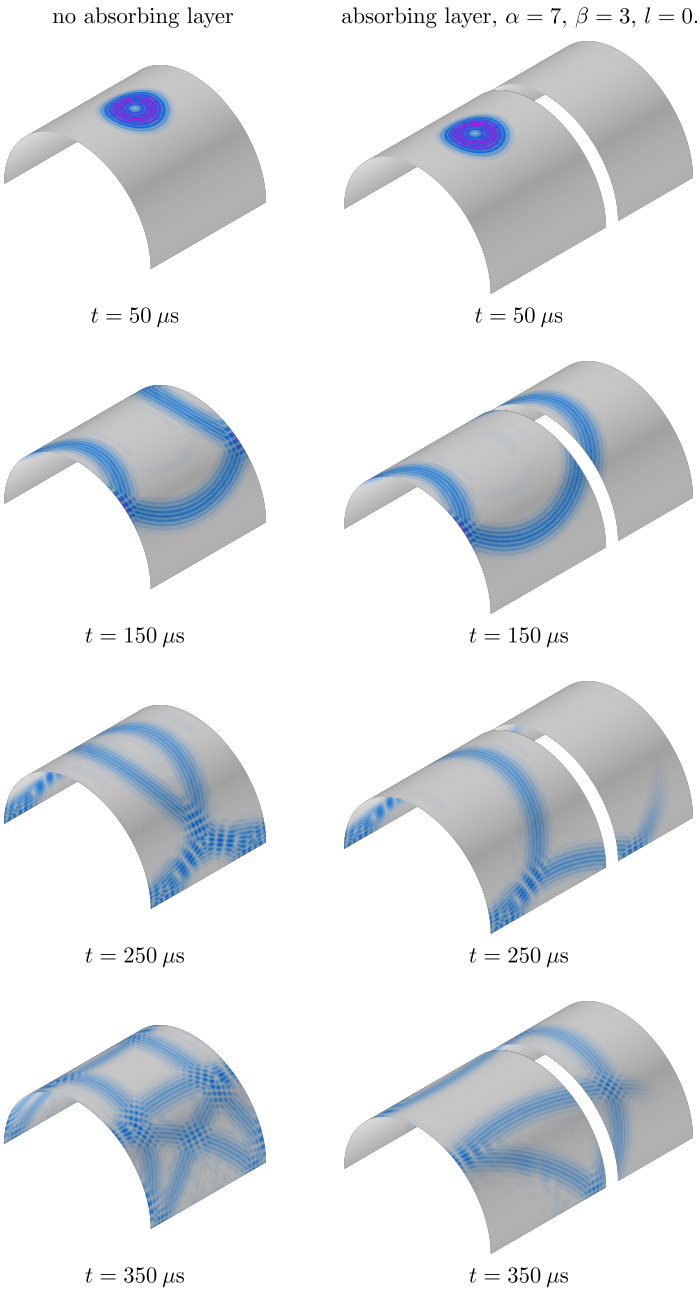

Figure 19: Wave propagation patterns within a 3-D isotropic half-pipe shell without or with an absorbing layer ($\alpha = 7, \beta = 3, l = 0.32$ m).

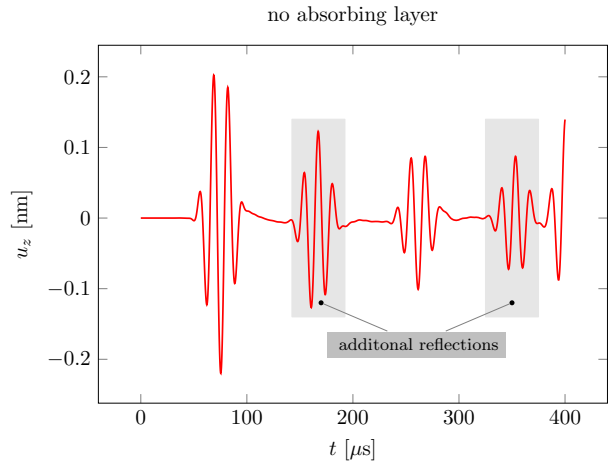

Figure 20: Wave propagation patterns within an isotropic half-pipe without or with an absorbing layer ($\alpha = 7, \beta = 3, l = 0.32$ m).

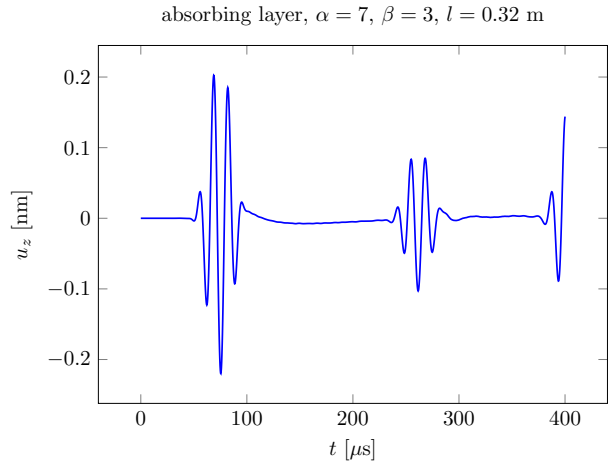

Figure 21: Wave propagation patterns within an isotropic half-pipe without or with an absorbing layer ($\alpha = 7, \beta = 3, l = 0.32$ m).

demanding due to the complexity of simulated phenomena as well as the geometrical properties of investigated structures. The concept of an absorbing layer with increasing damping (ALID) appears as a very good solution, especially when combined with such an effective numerical tool as the Time-domain Spectral Finite Element Method (TD-SFEM).

The results presented in this work allow the authors to formulate certain conclusions about the application and effectiveness of the ALID in the case of wave propagation related problems. The following conclusions can be drawn:

- It has been shown by the authors that the concept of the ALID can be effectively combined with the TD-SFEM.
- It has been demonstrated numerically by use of the TD-SFEM that the ALID can be applied in order to mimic semi-infinite boundary conditions in the case of wave propagation problems in 1-D rod, beam and 3-D shell structures.
- In the opinion of the authors, and based on the results obtained, it can be stated that the application of the ALID can also be successfully extended onto problems related with infinite boundary conditions as well as other types of 1-D, 2-D or 3-D structures.
- The properties of the ALID should always be closely correlated with the characteristics of propagating elastic waves.
- The length of the ALID should be selected as close to the length or double the length of the longest waves propagating in the structure.
- It is suggested by the authors that for the ALID lengths equal to the longest length of propagating elastic waves the values of the α and β parameters are selected as equal to 6 and 1, respectively.
- However, it is recommended by the authors to use layers of the lengths equal to double the longest length of propagating elastic waves. In this case the values of the α and β parameters are selected as equal to 7 and 3, respectively.

5. Acknowledgements

The Authors of this work would like to gratefully acknowledge the support for their research provided by the Academic Computer Centre in Gdańsk. All results presented in this paper have been obtained by the use of the software available at the Academic Computer Center in Gdańsk.

References

[1] V. Giurgiutiu, Structural Health Monitoring with Piezoelectric Wafer Active Sensors, Academic Press, San Diego, 2007.

[2] D. Balageas, C.-P. Fritzen, A. Güemes, Structural Health Monitoring, Wiley-ISTE, London, 2006.

[3] W. Ostachowicz, P. Kudela, M. Krawczuk, A. Żak, Guided Waves in Structures for SHM. The Time-domain Spectral Element Method, John Wiley & Sons Ltd., Singapore, 2012.

[4] D. Komatitsch, J. Tromp, Spectral-element simulations of global seismic wave propagation – 1. validation, Geophysical Journal International 149 (2002) 390–412.

[5] J. Virieux et al., V. Etienne et al., V. Cruz-Atienza et al., Modelling seismic wave propagation for geophysical imaging, Seismic Waves – Research and Analysis 13 (2012) 253–304.

[6] A. Żak, M. Radzieński, M. Krawczuk, W. Ostachowicz, Damage detection strategies based on propagation of guided elastic waves, Smart Materials and Structures 21 (2012) doi:10.1088/0964–1726/21/3/035024.

[7] M. H. Soorgee, C. J. Lissenden, J. L. Rose, A. Yousefi-Koma, Planar guided waves for shm of plate structures using piezoelectric fiber transducers, AIP Conference Proceedings 1511 (2013) 254–261.

[8] P. Bettess, Infinite Elements, Penshaw Press, Sunderland, 1992.

[9] A. J. Burton, G. F. Miller, The application of integral equation methods to the numerical solution of some exterior boundary-value problems, Proceedings Royal Society London A 323 (1971) 201–210.

[10] D. Givoli, J. B. Keller, Non-reflecting boundary conditions for elastic waves, Wave Motion 12 (1990) 261–279.

[11] J. Sochacki, R. Kubichek, J. George, W. R. Fletcher, S. Smithson, Absorbing boundary condition and surface waves, Geophysiscs 52 (1987) 60–71.

[12] G. Liu, J. S. Quek, A non-reflecting boundary for analysis wave propagation using the finite element method, Finite Elements in Analysis and Design 39 (2003) 403–417.

[13] M. B. Drozdz, Efficient finite element modelling of ultrasound waves in elastic media. Ph.D. Thesis, Imperial College of Science Technology and Medicine. University of London, London, 2008.

[14] C. B. Zhao, Coupled method of finite and dynamic infinite elements for simulating wave propagation in elastic solids involving infinite domains, Science China Technological Sciences 53 (2010) 1678–1687.

[15] L. Cremers, K. R. Fyfe, On the use of variable order infinite wave envelope elements for acoustic radiation and scattering, Acoustical Society of America 97 (1995) 2028–2040.

[16] A. Baghbani, D. Gregory-Smith, A new infinite element for unbounded water wave problems, Applied Ocean Research 25 (2003) 213–223.

[17] R. J. Astley, J. A. Hamilton, The stability of infinite element schemes for transient wave problems, Computer Methods in Applied Mechanics and Engineering 3553–3571 (2006) 195.

[18] Y. B. Yang, H. H. Hung, D. W. Chang, Train-induced wave propagation in layered soils using finite/infinite element simulation, Soil Dynamics and Earthquake Engineering 23 (2003) 263–278.

[19] D. Givoli, Higher-order local non-reflecting boundary conditions: a review, Wave Motion 39 (2004) 319–326.

[20] J. P. Berenger, A perfectly matched layer for the absorption of electromagnetic waves, Journal of Computational Physics 114 (1994) 185–200.

[21] J. P. Berenger, Three-dimensional perfectly matched layer for the absorption of electromagnetic waves, Journal of Computational Physics 127 (1996) 363–379.

[22] Q. Qi, T. L. Geers, Evaluation of the perfectly matched layer for computational acoustics, Journal of Computational Physics 139 (1998) 166–183.

[23] D. Komatitsch, J. Tromp, A perfectly matched layer absorbing boundary condition for the second-order seismic wave equation, Geophysical Journal International 154 (2003) 146–153.

[24] J. Kristek, P. Moczo, M. Galis, A brief summary of some pml formulations and discretizations for the velocity-stress equation of seismic motion, Studia Geophysica et Geodaetica 53 (2009) 459–474.

[25] F. D. Hastings, J. B. Schneider, S. L. Broschat, Application of the perfectly matched layer (pml) absorbing boundary conditions to elastic wave propagation, Journal of Acoustical Society of America 100 (1996) 3061–3069.

[26] R. M. Song, W. K. Ma, The application of the nonsplitting perfectly matched layer in numerical modeling of wave propagation in poroelastic media, Applied Geophysics 2 (2005) 216–222.

[27] F. Nataf, New constructions of perfectly matched layers for the linearized euler equations, Comptes rendus – Mathematiques 340 (2005) 775–778.

[28] M. Israeli, S. A. Orszag, Approximation of radiation boundary conditions, Journal of Computational Physics 41 (1981) 115–135.

[29] A. Modave, E. Deleersnijder, J. M. Éric, On the parameters of absorbing layers for shallow water models, Ocean Dynamics 60 (2010) 65–79.

[30] S. H. Kim, B. Kwang-Jin, E. Scott, Analysis of wave propagation in saturated porous media. ii. parametric studies, Computer Methods in Applied Mechanics and Engineering 191 (2002) 4075–4091.

[31] A. Żak, M. Krawczuk, Assessment of rod behaviour theories used in spectral finite element modelling, Journal of Sound and Vibration 329 (2010) 2099–2113.

[32] A. Żak, M. Krawczuk, Assessment of flexural beam behaviour theories used for dynamics and wave propagation problems, Journal of Sound and Vibration 331 (2012) 5715–5731.

[33] A. Żak, A novel formulation of a spectral plate element for wave propagation in isotropic structures, Finite Elements in Analysis and Design 45 (2009) 650–658.

[34] O. C. Zienkiewicz, The Finite Element Method, McGraw-Hill Book Company, London, 1989.